ARMY RESEARCH LABORATORY

A Piezoelectric MEMS Microphone Based on Lead Zirconate Titanate (PZT) Thin Films

by Ronald G. Polcawich

ARL-TR-3387 **November 2004**

NOTICES

Disclaimers

The findings in this report are not to be construed as an official Department of the Army position unless so designated by other authorized documents.

Citation of manufacturer's or trade names does not constitute an official endorsement or approval of the use thereof.

Destroy this report when it is no longer needed. Do not return it to the originator.

Army Research Laboratory
Adelphi, MD 20783-1197

ARL-TR-3387 **November 2004**

A Piezoelectric MEMS Microphone Based on Lead Zirconate Titanate (PZT) Thin Films

Ronald G. Polcawich
Sensors and Electron Devices Directorate, ARL

REPORT DOCUMENTATION PAGE

Form Approved
OMB No. 0704-0188

1. REPORT DATE *(DD-MM-YYYY)*	2. REPORT TYPE	3. DATES COVERED (From - To)
November 2004	Final	December 2002 to July 2004

4. TITLE AND SUBTITLE
A Piezoelectric MEMS Microphone Based on Lead Zirconate Titanate (PZT) Thin Films

5a. CONTRACT NUMBER

5b. GRANT NUMBER

5c. PROGRAM ELEMENT NUMBER

6. AUTHOR(S)
Ronald G. Polcawich

5d. PROJECT NUMBER

5e. TASK NUMBER

5f. WORK UNIT NUMBER

7. PERFORMING ORGANIZATION NAME(S) AND ADDRESS(ES)
U.S. Army Research Laboratory
ATTN: AMSRD-ARL-SE-RL
2800 Powder Mill Road
Adelphi, MD 20783-1197

8. PERFORMING ORGANIZATION REPORT NUMBER
ARL-TR-3387

9. SPONSORING/MONITORING AGENCY NAME(S) AND ADDRESS(ES)
U.S. Army Research Laboratory
2800 Powder Mill Road
Adelphi, MD 20783-1197

10. SPONSOR/MONITOR'S ACRONYM(S)

11. SPONSOR/MONITOR'S REPORT NUMBER(S)

12. DISTRIBUTION/AVAILABILITY STATEMENT
Approved for public release; distribution unlimited.

13. SUPPLEMENTARY NOTES

14. ABSTRACT
Piezoelectric microelectromechanical (MEMS) scale acoustic sensors have potential applications in a wide variety of applications including hearing aids, surveillance, and heart monitoring. For each of these systems and many others, the acoustic sensors must be miniaturized and have low power requirements. A piezoelectric-based microphone can provide a solution to these requirements, since it offers the ability to passively sense without the power requirements of condenser or piezoresistive microphone counterparts. This research effort reports on the design and fabrication of a piezoelectric $PbZr_{0.52}Ti_{0.48}O_3$ (PZT) based acoustic sensor. A circular clamped membrane consisting of a dielectric for structural support and a piezoelectric actuator has been fabricated on a silicon wafer via silicon deep reactive ion etching (DRIE). Sensors ranging from 500 to 2000 microns in diameter have been fabricated and characterized with the use of scanning laser Doppler vibrometry and calibrated acoustic tone sources. The PZT sensors exhibited a sensitivity of 97.9 to 920 nV/Pa, depending on geometry.

15. SUBJECT TERMS
PZT, acoustic Sensor, MEMS, microphone

16. SECURITY CLASSIFICATION OF:			17. LIMITATION OF ABSTRACT	18. NUMBER OF PAGES	19a. NAME OF RESPONSIBLE PERSON
a. REPORT	b. ABSTRACT	c. THIS PAGE			Ronald G. Polcawich
Unclassified	Unclassified	Unclassified	UL	28	19b. TELEPHONE NUMBER (*Include area code*) (301) 394-1275

Standard Form 298 (Rev. 8/98)
Prescribed by ANSI Std. Z39.18

Contents

List of Figures

List of Tables

INTENTIONALLY LEFT BLANK.

1. Introduction

Miniature acoustic sensors are crucial for a wide range of military and commercial applications. A microelectromechanical (MEMS) scale acoustic sensor can easily be implemented into a sensor suite used for unattended remote sensing applications or as an inexpensive hearing aid for the hearing impaired. Other potential applications include use in acoustic signal localization, physiological monitoring, and as an integral component in a MEMS scale photoacoustic spectrometer.

There have been numerous efforts in developing a MEMS microphone. The three main approaches investigated have been capacitive, piezoresistive, and piezoelectric (*1-7*). Most past research has focused on complementary metal oxide semiconductor (CMOS) integration so that on-chip amplifier circuitry can be implemented along with the microphone. Capacitive and resistive microphones have been examined the most because of their relative ease integrating with microelectronics. Additionally, substantial efforts have been put forth attempting to integrate a zinc oxide (ZnO) piezoelectric microphone with CMOS (*8-10*).

Table 1 illustrates several performance specifications for the three main microphone technologies. A piezoelectric-based microphone can offer two main advantages: no required input power and a wide dynamic range. A passive acoustic sensor is ideal for the low cost, disposable sensors required by the military for remote sensing. Although the piezoelectric sensors may be less sensitive than their capacitive and piezoresistive counterparts, they can be very advantageous in situations not necessarily governed by sensor sensitivity. For example, in an open environment, low frequency, 1/f noise, can dominant the spectrum and provide a noise floor of 30 to 40 dB sound pressure level (SPL) (re 20 μPa). During the same conditions, typical battlefield sounds can be much greater than 100 dB SPL (e.g., a brick of C4 explosive at 30 m is 165 dB and a rifle shot at the shooter's ear is 156 dB).

Table 1. Basic performance characteristics of the three most investigated MEMS microphones (*1*).

	Capacitive	**Piezoresistive**	**Piezoelectric**
Sensitivity (◊V/Pa)	Good 400 to 1000	Low 0.1 to 100	Medium 10 to 500
Input Power	Required	Required	None
Dynamic Range	Narrow	Relatively Wide	Wide

For a passive piezoelectric microphone, there are several options for the thin film sensor material including ZnO, aluminum nitride (AlN), and lead zirconate titanate (PZT). Our research focused on developing a PZT microphone because of its large piezoelectric coefficient and low dielectric loss compared to ZnO. The microphone was designed for use in a MEMS scale photoacoustic spectroscopy system (*11*,*12*). The MEMS microphone was integral in the miniaturization of the photoacoustic resonant cell allowing for improved trace gas sensing through a reduction in path length between the photoacoustic event and the acoustic sensor (see figure 1).

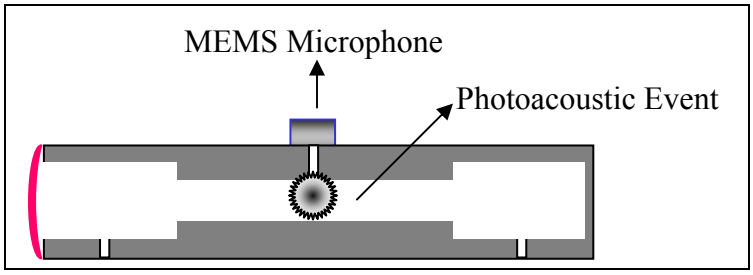

Figure 1. Schematic description of a MEMS photoacoustic resonant cell.

A general comparison of ZnO and PZT thin films is available in table 2. With a rudimentary equation for microphone sensitivity, it is quite clear that a microphone using PZT will not yield the most sensitive microphone. Although PZT has a transverse piezoelectric coefficient an order of magnitude larger than ZnO, the gain in performance is reduced because of its 100-fold increase in dielectric constant. One potential benefit of using PZT over ZnO is the lower dielectric loss typically exhibited in PZT. With this understanding, this report outlines the research to date on the development of PZT MEMS microphone for potential use in a prototype MEMS photoacoustic spectrometer and for use as a remote acoustic sensor.

Table 2. ZnO (*13*) and PZT thin film properties and microphone sensitivity.

	ZnO	**PZT**
Piezoelectric Coeffidient, d^{31} (pm/V)	-5	-50
Dielectric Constant	10	1000
Dielectric Loss	5 to 10%	2 to 4 %
Sensitivity (μV/Pa)	488	68

2. Microphone Fabrication

A piezoelectric microphone based on PZT thin films was designed in order to investigate its potential use as a passive sensing element in a photoacoustic resonant cell. The microphone fabrication process began with a double-sided polished silicon wafer and used several different types of deposition systems (see figure 2). A plasma-enhanced chemical vapor-deposited (PECVD) silicon dioxide thin film (1 μm thick) was deposited with a Plasma-Therm 790 reactor using a mixture of SiH_4, He, and N_2O. The oxide served as the membrane structural layer and was chosen to be 1 μm thick. After deposition, the film was annealed in an A.G. Associates Heatpulse 610 rapid thermal anneal (RTA) furnace at 700 °C for 60 seconds in a nitrogen atmosphere. This annealing removes the trapped hydrogen within the film and causes the film to obtain a slightly tensile stress, which aids in producing a planar membrane and a high performance microphone.

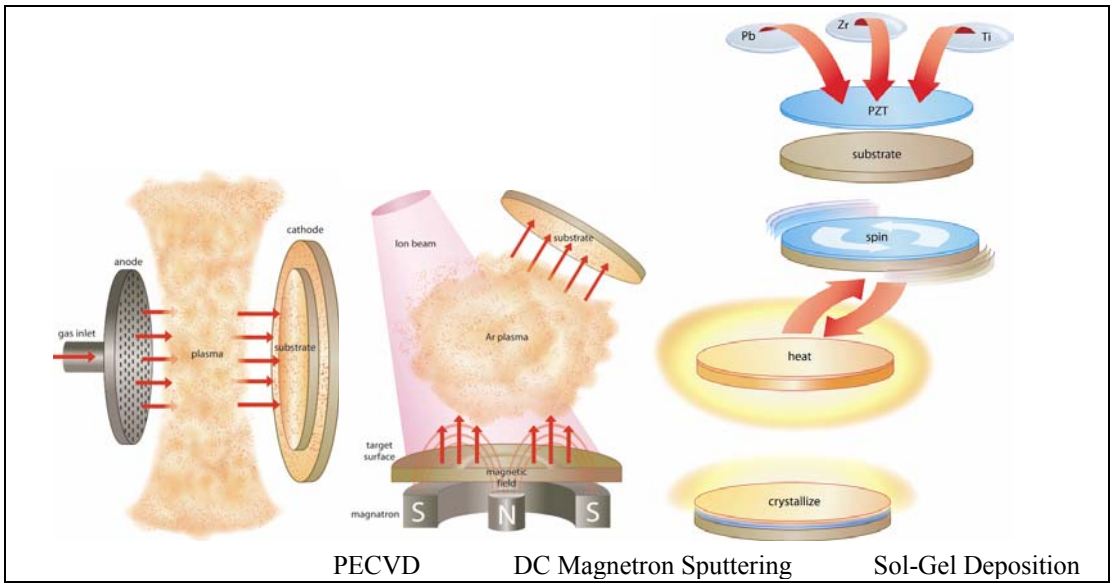

Figure 2. Processes for the deposition of (a) PECVD dielectrics, (b) DC magnetron sputtered metals, and (c) sol-gel deposited PZT thin films.

After the oxide is deposited and annealed, a metal electrode was deposited via sputtering to serve as the bottom electrode and as a growth template for the piezoelectric actuator. For adhesion to the oxide, a thin layer (200 Å) of titanium was first sputtered and was immediately followed by platinum deposition (800 Å) without breaking vacuum within a Varian 3190 direct current (DC) magnetron sputter deposition system. Following the platinum deposition, the wafers were annealed in the RTA furnace at 700 °C for 60 seconds in flowing dry air in order to improve the adhesion between the oxide and metal layers and the surface texture of the platinum before deposition of the piezoelectric thin film.

The next fabrication step was to deposit the $PbZr_{0.52}Ti_{0.48}O_3$ thin film. The deposition process is a solution spin on process. First, a PZT sol-gel solution was prepared via a modified alkoxide process first introduced by Budd, Dey, and Payne (*14*). This process used lead acetate trihydrate, zirconium n-propoxide, and titanium isopropoxide as the precursors and 2-methoxyethanol as the solvent. Once the sol-gel solution was prepared and aged, the repetitive deposition process, as depicted in figure 3c, began with a portion of the sol dispensed onto a platinized silicon substrate. The wafer was then spun at 2,500 rpm for 30 seconds. Next, the wafers were placed onto a hotplate at 350 °C for 120 seconds, which causes the film to undergo pyrolysis, thereby decomposing all the organics. This process of deposition, spin, and pyrolysis was then repeated a total of four times. After the last pyrolysis, the wafer was annealed in a RTA furnace at 700 °C for 30 seconds in flowing air in order to crystallize the PZT thin film. The result was approximately a 0.25 μm PZT film, and the entire process was continued in order to achieve the desired thickness of a 1-μm PZT thin film.

After the piezoelectric was deposited, a top electrode of platinum (800 Å) was sputter deposited onto the wafer surface. The wafers were then annealed in an RTA at 350 °C for 120 seconds in flowing air to improve adhesion and reduce any sputtering induced surface damage.

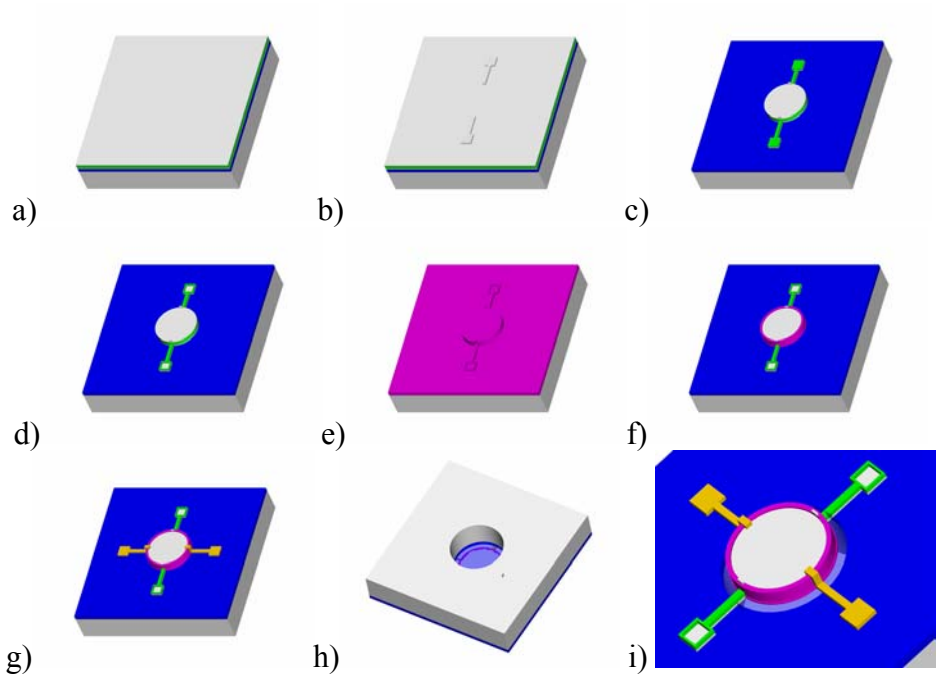

Figure 3. Fabrication process flow for creating a PZT membrane microphone: (a) Starting wafer, (b) sacrificial titanium, (c) Ar ion mill of Ti/Pt/PZT/Pt, (d) PZT wet etch, (e) oxide passivation deposition, (f) etching of passivation, (g) Ti/Au contact, (h) silicon DRIE, and (i) front view of released PZT membrane.

The resultant wafer stack at this stage is $Si/SiO_2/Ti/Pt/PZT/Pt$. The first step in the microphone fabrication is to define the final actuator dimensions and the location of the electrical contacts. Because electrical contact has to be made with the bottom Ti/Pt electrode, a sacrificial titanium layer was electron beam evaporated onto the wafer and patterned with a lift-off technique. The next step was to pattern the wafer with Clariant AZ 5214E reverse image photoresist. To define the final actuator dimensions, argon ion milling was employed to sputter remove the Ti/Pt/PZT/Pt stack from most of the wafer. During this process, the sacrificial Ti layer will prevent the ion milling of approximately half the PZT layer and all of the Ti/Pt bottom electrode.

After removal of the photoresist, another resist pattern was placed onto the wafer in order to open windows to the bottom electrode. Within these windows, the structure was $Si/SiO_2/Ti/Pt/PZT$. The PZT was then wet etched with H_20:HCl:HF (2:1:0.02) in order to expose the Pt. Afterwards, the photoresist was removed with photoresist stripper at 85 °C.

The next step in the fabrication was to deposit a 2500-Å PECVD SiO_2 thin film to serve as an isolation layer preventing electrical contact between the top and bottom electrical traces. After deposition, the film was annealed in an RTA at 350 °C for 120 seconds in flowing N_2 and then again for 120 seconds in flowing air. This anneal improves the adhesion between the structural silicon dioxide and the isolation oxide. The next step was to pattern the oxide around the circumference of the actuator. Again, positive photoresist was used and the wafer was placed into a LAM[1] 590 etching system in which the oxide was etched with CHF_3/CF_4 plasma.

To make electrical contact with the top Pt electrode of the actuator, an evaporated 200-Å Ti/ 2500 Å Au layer was deposited and patterned with a lift-off technique. The Ti/Au was also deposited onto the bottom Ti/Pt electrode so that gold wire bonding could be used to package the final devices.

The final fabrication step was a deep reactive ion etch (DRIE) of the silicon substrate in order to release the membrane actuator. With a Karl-Suss MA/BA[1] 6 mask aligner, a 6-μm thick positive photoresist (AZ 9245) was patterned onto the reverse side of the silicon substrate. The silicon DRIE was performed with a Unaxis VLR[1] cluster tool configured with an inductively coupled plasma (ICP) etch chamber. The silicon DRIE followed the Bosch (*15*) process using a cyclical etching process that consisted of a polymer deposition with a C_4F_8 plasma followed by an isotropic silicon etching with a SF_6 plasma. In addition to creating a released membrane, the Bosch etch was used to separate each of the device die (see figure 4).

[1] not an acronym.

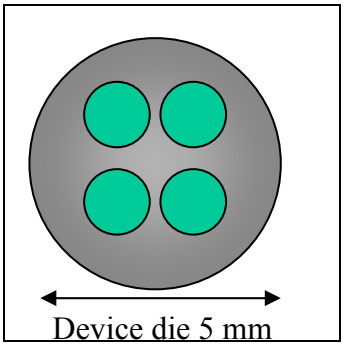

Figure 4. Illustration of the device die, after the Bosch process, with as many as four individual PZT microphones per die.

After etching, the remaining photoresist was removed with an oxygen plasma, and the resultant microphone die were ready for packaging. The separated device die were subsequently packaged with a TO-8 package that was pre-drilled with a circular release hole. The release hole allows the membrane to deflect and freely push air out the opening, thereby reducing the deleterious effect of squeeze film damping.

3. Acoustic Testing

We evaluated the performance of a PZT microphone by placing a packaged microphone die into an electrical test chamber (as seen in figure 5) with rubber grommet seals to prevent outside noise interference. An acrylic cap was placed on top the packaged microphone die, and a Tygon[2] tube was attached between the acrylic cap and the tube driver assembly. The acoustic test chamber was configured with BNC[3] mounts for electrical connection and a 1/8-inch inner diameter (ID) nozzle for connecting to the Tygon tube from the signal source.

[2] Tygon® is a registered trademark of Saint Gobain Performance Plastics.

[3] not an acronym.

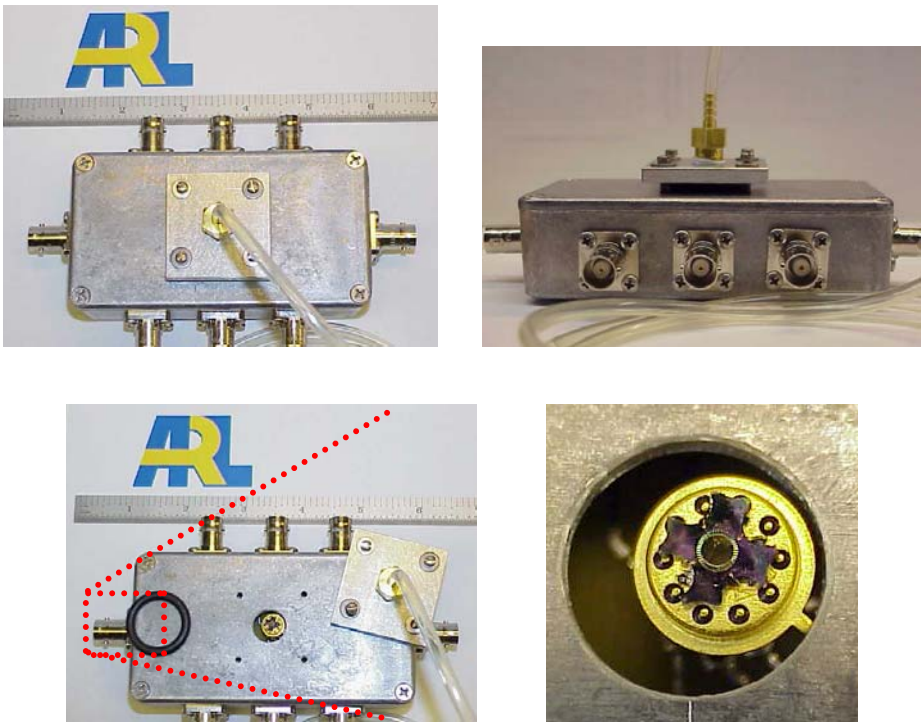

Figure 5. Images of the acoustic test chamber used for testing the PZT microphone. (The BNC mounts provide electrical contact to the packaged microphone whereas the acrylic plate on top provides a connection for the acoustic tube.)

Two different sound sources were used to characterize the performance of the PZT microphones. The first source was an ACO[4] Pacific electromagnetic source outputting a 1-kHz tone of either 94 dB or 104 dB. The second sound source was a B&K[4] Pistonphone producing a 124-dB tone at either 250 Hz or 325 Hz. As seen schematically in figure 6, the generated acoustic wave was detected simultaneously by both a B&K[4] calibrated microphone and the PZT microphone. The data were collected with Labview software and subsequently analyzed with a MATLAB[5] algorithm. To improve output signal from the PZT microphones, a Stanford Research Systems 4330 operational amplifier was added during the measurements.

[4] not an acronym.

[5] MATLAB® is a registered trademark of the Math Works.

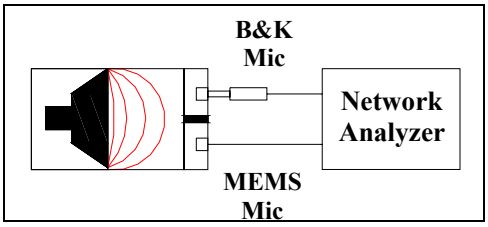

Figure 6. Schematic representation of experimental test setup for analysis of the PZT and calibrated B&K microphones.

4. Results and Discussion

PZT membrane microphones with a diameter from 500 to 2000 μm were successfully fabricated with two main designs initially focused upon. The first consisted of a PZT sensor covering the central 80% of the released diaphragm while the second consisted of a PZT sensor covering the outer 20% of the released diaphragm (see figures 7a and 7b, respectively). By reducing the coverage of the PZT, a maximum output signal can be obtained by the combination of the contribution from conflicting strain responses of a deflecting membrane. The 80/20 break down of the two microphones was chosen because the inflection point in the strain response of a deflecting membrane lies near this location. For each of the two choices, the PZT has been removed from outside the sensor region.

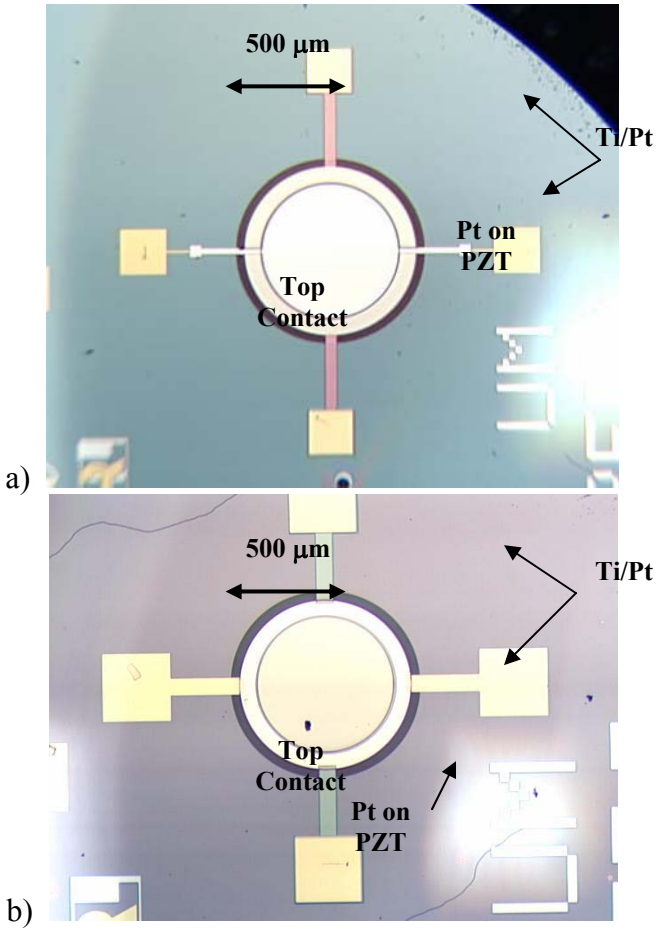

Figure 7. (a) Optical surface micrograph of a PZT membrane actuator with center 80% electroded and (b) optical surface micrograph of a PZT actuator with outer 20% electroded.

Scanning electron micrographs in figure 8a illustrate the Bosch etch used to create the released membrane. The resultant membrane structure consists of an overall positive stress gradient resulting in a planar released surface as depicted in figure 8b. The bumps on the surface of the device die are the remnant gold wire bonds. The last image in figure 8 shows the oxide passivation around the perimeter of the PZT sensor as well as the Ti/Au contact strap.

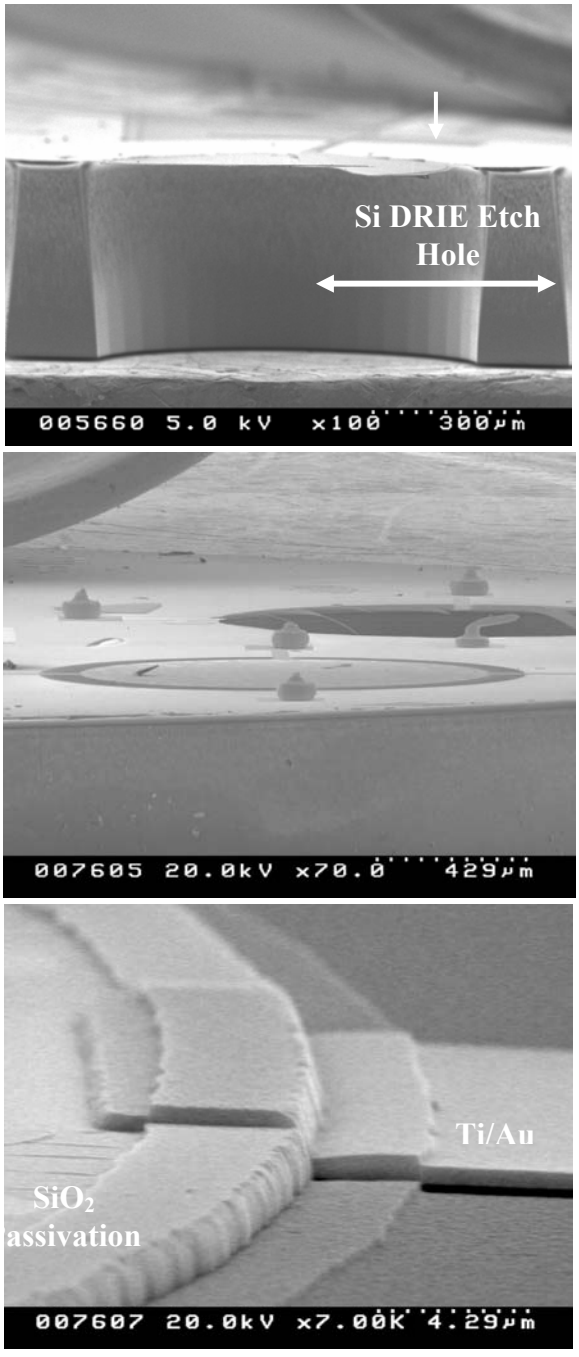

Figure 8. (a) An SEM image of a silicon DRIE release, (b) SEM image of the surface profile of a released membrane, and (c) SEM image illustrating the SiO_2 passivation.

To assess the performance of the PZT membranes, the packaged die were first analyzed with a Polytec scanning laser Doppler vibrometer so that the resonance characteristics could be obtained. With a pseudorandom 1-$V_{p\text{-}p}$ input signal with a 1-V_{offset}, the frequency response and resonant mode shapes can be obtained for each of the diaphragms tested (see figure 9). Testing of various sized membranes confirmed that when driven as actuators, they exhibit a classic 1/r frequency dependence, in which r is the membrane radius, thereby proving that the microphones operate as membranes and not as clamped plates (see figure 10).

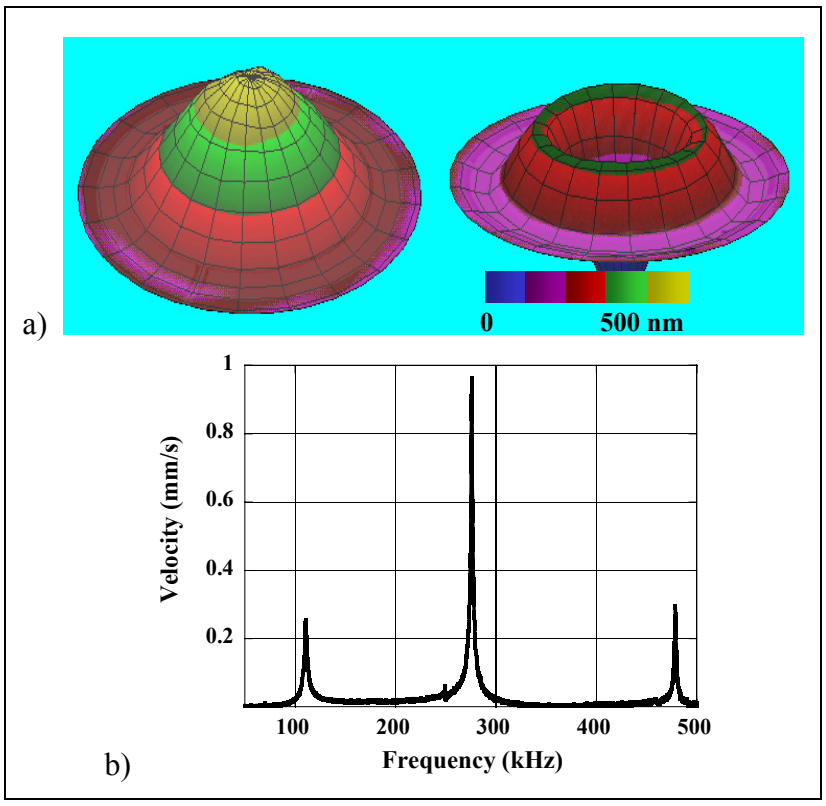

Figure 9. Laser Doppler vibrometry (LDV) results (a) mode shapes of fundamental and third harmonic vibration and (b) frequency response from a 500-μm diameter membrane with 80% sensor coverage.

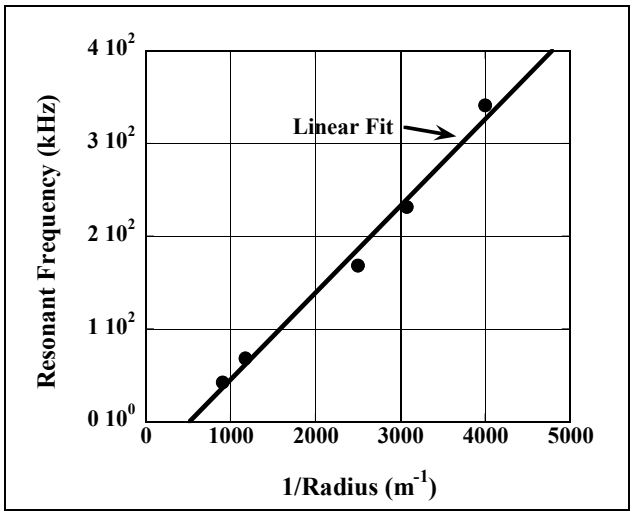

Figure 10. Resonant frequency versus the inverse membrane radius confirming membrane behavior rather than clamped plate behavior of the PZT microphones.

The acoustic response of the microphones was plotted on a power (dB·V) versus frequency plot after a fast Fourier transform (FFT) was performed on the voltage output from each sensor. Typical plots generated for both sound sources are seen in figures 11a and 11b for a 750-μm diameter microphone with 20% sensor coverage. The PZT microphones performed well in these early experiments with magnitudes not too dissimilar from the B&K microphone. A clear distinction between the PZT and B&K output was the amount of noise in the PZT response. One side effect of using an unmatched amplifier was the unintentional amplification of the noise in both the data acquistion as well as chamber losses. The noise amplification was also evident in the 60 Hz harmonics present in figure 11 at 300 Hz and 1020 Hz. Although the noise floor is amplified, it remains in the low to mid 10^{-6} V range whereas the noise floor for the B&K microphone is 10^{-7} V.

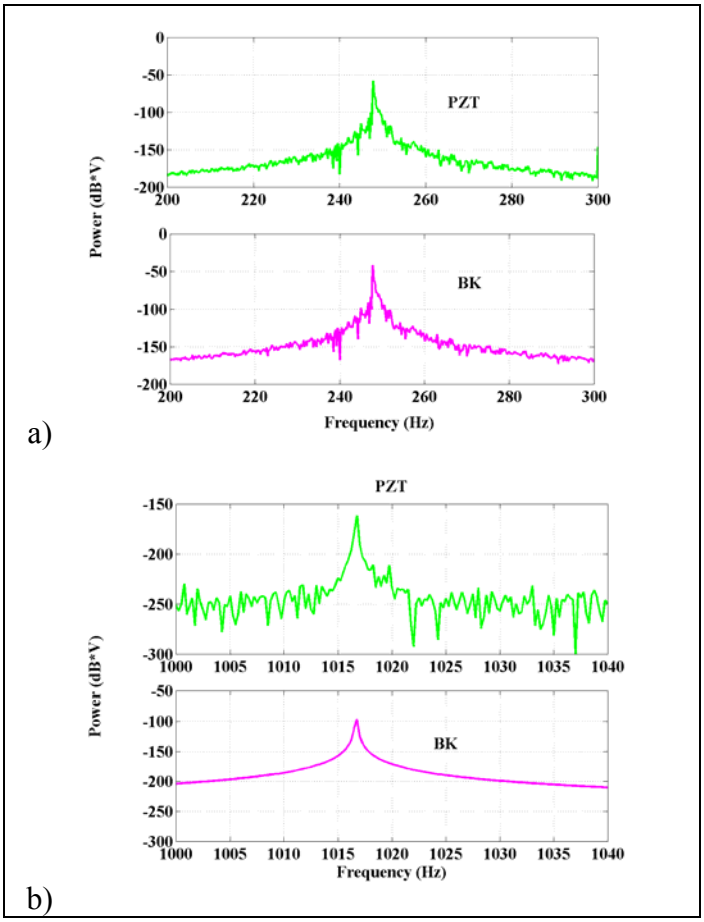

Figure 11. Acoustic response of a B&K and a 750-µm diameter PZT MEMS microphone with 20% sensor coverage for (a) B&K Pistonphone 250-Hz tone at 124 dB and (b) ACO Pacific 1-kHz tone at 104 dB.

An examination of the acoustic output from the PZT microphone produced an unamplified sensitivity of 97.9 to 920 nV/Pa, depending on the size and configuration of the microphone. This sensitivity falls far short from the predicted values that should range in the mid to high microvolt per Pascal. The plot in figure 12 compares the predicted sensitivities against the experimentally determined values including the amplifier. The amplified sensitivities were plotted for ease of viewing both values. Each curve follows a radius squared relationship as expected from the area term in the sensitivity equation. Unfortunately, the experimental values do not possess the same multiplicative constant for increasing radius. Even with low sensitivities of the PZT microphone, they exhibit a current limit of detection of ~ 50 dB SPL, which can make the sensor viable as a remote acoustic sensor and useful in the preliminary testing of a MEMS photo-acoustic sensor.

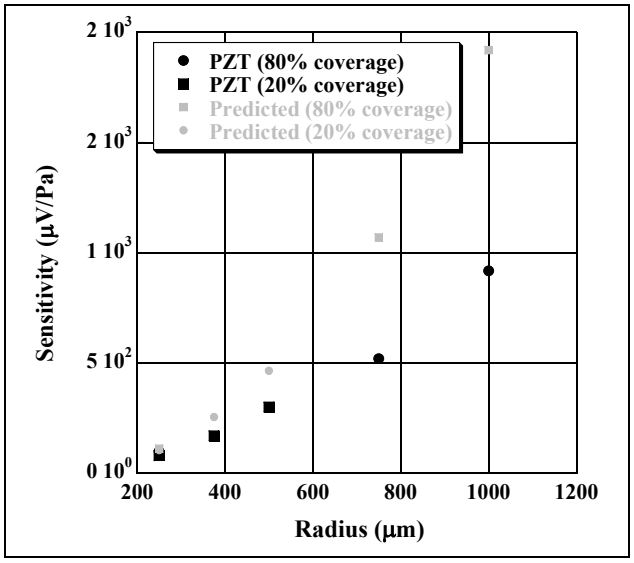

Figure 12. Sensitivity versus radius of microphone including both predicted values and the amplified experimental results for the 20% and 80% coverage sensors.

There are several potential possibilities for the difference between predicted and experimental values. One important characteristic to the predicted values concerns the assumption of zero residual stress. It is well known from previous research efforts that a composite PZT thin film actuator possesses a wide variety of residual stress values with the overall gradient determining the behavior of the final device. As previously stated with figure 7, a planar-released membrane indicates a positive residual stress gradient in the composite. In addition to the residual stress assumption, the sensitivity equation also assumes a minimal load capacitance. There is definitely a finite load capacitance in the electrical setup, especially considering the impedance mismatch between the PZT sensor and the SRS operational amplifier (op-amp) and the extraordinarily long connection cables. The final assumption with the sensitivity equation is proper match of both the acoustic and electrical domains. Even though there is a open cavity in the TO-5 package, there is an acoustic mismatch between the DRIE release via hole and the open air cavity of the test chamber.

Another possible reason for the diminished output from the PZT microphones was resolved upon investigation of the dielectric and ferroelectric properties of the devices. The dielectric properties of the microphones were good with dielectric constants of 1021 ± 55 and a dielectric loss of 3.5% ± 1%. Unfortunately, the ferroelectric hysteresis loops exhibited a pinched hysteresis loop indicative on a non-optimal PZT thin film and may lead to diminished piezoelectric properties (see figure 13). It is true that some of the normal hysteretic response can be achieved with poling but in order to fully remove the effect of the pinched loop, a thermal poling process is required. The packaged microphones were unable to undergo a thermal poling process due at the time of this investigation.

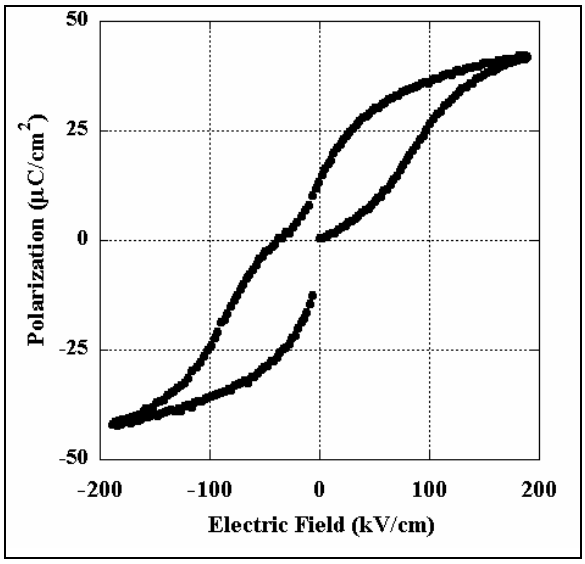

Figure 13. Abnormal polarization electric field hysteresis loop for a 1000-μm diameter PZT microphone.

Besides optimizing the material properties and the acoustic and impedance matches, one possibility for increasing the sensitivity is using electrode shaping and/or design. Combining the output signal from the inner and outer regions of a deflecting membrane can be extremely beneficial to the performance of a membrane. As presented by Kim (*9*), differential summation from different regions of the acoustic sensor can be used to optimize the voltage output from a piezoelectric microphone while minimizing the effects of increased capacitance with sensor size. Our first attempts examine the combined output from a PZT sensor with both the outer 20% and inner 75% covered with PZT (see figure 14).

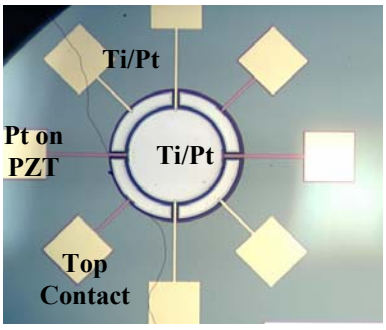

Figure 14. Optical micrograph of a 80/20 combined acoustic sensor.

5. Conclusion

Initial research successfully fabricated a piezoelectric microphone for acoustic sensing. The PZT microphones were shown to perform well up to their mechanical resonant frequency and may provide a low power means of detecting acoustic signals. These initial microphones exhibit a sensitivity of 97.9 to 920 nV/Pa. Although these values are lower than predicted performance, further modifications of the microphone, acoustic and electric impedance matching, and predicting equations were presented as a means to further enhance the development of a PZT MEMS-based microphone.

6. References

1. Scheeper, P. R.; van der Donk, A.G.H.; Olthuis, W.; Bergveld, P. A Review of Silicon Microphones. *Sens. Act. A* **1994**, *44*, 1-11.

2. Fraim, F. W.; Murphy, P. V. Miniature Electret Microphones. *J. Audio Eng. Soc.* **1970**, *18*, 511-7.

3. Hohm, D.; Hess, G. A Subminiature Condenser Microphone with Silicon Nitride Meembran and Silicon Back Plate. *J. Acoust. Soc. Am.* **1989**, *85*, 476-80.

4. Sprenkels, A. J.; Groothengel, R. A.; Verloop, A. J.; Bergveld, P. Development of an Electret Microphone in Silicon. *Sens. Act A* **1989,** *17*, 509-12.

5. Schellin, R.; Hess, G. A Silicon Subminiature Microphone based on Piezoresistive Polysilicon Strain Gauges. *Sens. Act. A* **1992**, *32*, 555-9.

6. Shellin, R.; Strecker, M.; Nothelfer, U.; Schuster, G. Low Pressure Acoustic Sensors for Airborne Sound with Piezoresitive Monocrystalline Silicon and Electrochemically Etched Diaphragms. *Sens. Act. A* **1995**, *46-7*, 156-60.

7. Arnold, D.; Gururaj, S.; Bhardwaj, S.; Nishida, T.; Sheplak, M. A Piezoresisitive Microphone for Aeroacoustic Measurements. *Proc. 2001 ASME Intern. Mech. Eng. Cong. Expos.*, New York, Nov. 2001.

8. Royer, M.; Holmen, J. O.; Wurm, M. A.; Aadland, O. S.; Glenn, M. ZnO on Si Integrated Acoustic Sensor. *Sens. Act. A.* **1983**, *4*, 357-62.

9. Kim, E. S. Integrated Microphone with CMOS circuits on a Single Chip. Ph. D dissertation, EECS Dept., Univ. of Cal., Berkeley, May 1990.

10. Reid, R.; Kim, E.; Hong, D.; Muller, R. Piezoelectric Microphone with On-Chip CMOS Circuits. *J. MEMS* **1993**, *2*, 111-20.

11. Pellegrino, P.; Polcawich, R. Advancement of a MEMS Photoacoustic Chemical Sensor. submitted to *SPIE Aerosense Chemical and Biological Sensing IV* **2003**, *5085.*

12. Pellegrino, P.; Polcawich R. Evaluation of a MEMS Photoacoustic Sensor. submitted to 2002 Joint Service Scientific Conference Chemical Biological Defense Research, Hunt Valley.

13. http://www.memsnet.org/material/zincoxideznofilm/

14. Budd, K. D.; Dey, S. K.; Payne, D. A. Sol-Gel Processing of PbTiO3, PbZrO3, PZT, and PLZT Thin Films. *Brit. Cer. Proc.* **1985**, *36*, 107-21.

15. Laermer, F.; Schilp, A. Method of Anisotropically Etching Silicon. US-Patent No. 55018893.

Distribution List

ADMNSTR
DEFNS TECHL INFO CTR
ATTN DTIC-OCP (ELECTRONIC COPY)
8725 JOHN J KINGMAN RD STE 0944
FT BELVOIR VA 22060-6218

DARPA
ATTN IXO S WELBY
3701 N FAIRFAX DR
ARLINGTON VA 22203-1714

OFC OF THE SECY OF DEFNS
ATTN ODDRE (R&AT)
THE PENTAGON
WASHINGTON DC 20301-3080

US MILITARY ACDMY
MATHEMATICAL SCI CTR OF EXCELLENCE
ATTN LTC T RUGENSTEIN
THAYER HALL RM 226C
WEST POINT NY 10996-1786

SMC/GPA
2420 VELA WAY STE 1866
EL SEGUNDO CA 90245-4659

US ARMY ARDEC
ATTN AMSTA-AR-TD
BLDG 1
PICATINNY ARSENAL NJ 07806-5000

COMMANDING GENERAL
US ARMY AVN & MIS CMND
ATTN AMSAM-RD W C MCCORKLE
REDSTONE ARSENAL AL 35898-5000

HICKS & ASSOC INC
ATTN G SINGLEY III
1710 GOODRICH DR STE 1300
MCLEAN VA 22102

PALISADES INST FOR RSRCH SVC INC
ATTN E CARR
1745 JEFFERSON DAVIS HWY STE 500
ARLINGTON VA 22202-3402

DIRECTOR
US ARMY RSRCH LAB
ATTN AMSRD-ARL-RO-D JCI CHANG
ATTN AMSRD-ARL-RO-EN W D BACH
PO BOX 12211
RESEARCH TRIANGLE PARK NC 27709

US ARMY RSRCH LAB
ATTN AMSRD-ARL-CI-OK-T TECHL PUB (2 COPIES)
ATTN AMSRD-ARL-CI-OK-TL TECHL LIB (2 COPIES)
ATTN AMSRD-ARL-D J M MILLER
ATTN AMSRD-ARL-SE-RL
J PULSKAMP
ATTN AMSRD-ARL-SE-RL M DUBEY
ATTN AMSRD-ARL-SE-RL
P AMIRTHARAJ
ATTN AMSRD-AL-SE-RL
A WICKENDEN
ATTN AMSRD-AML-SE-RL E ZAKAR (10 COPIES)
ATTN AMSRD-ARL-SE-RL
L CURRANO
ATTN AMSRD-ARL-SE-RL
R POLCAWICH (10 COPIES)
ATTN IMNE-AD-IM-DR MAIL & RECORDS MGMT
ADELPHI MD 20783-1197

INTENTIONALLY LEFT BLANK.